NJC

Accepted Manuscript

This is an *Accepted Manuscript*, which has been through the Royal Society of Chemistry peer review process and has been accepted for publication.

Accepted Manuscripts are published online shortly after acceptance, before technical editing, formatting and proof reading. Using this free service, authors can make their results available to the community, in citable form, before we publish the edited article. We will replace this *Accepted Manuscript* with the edited and formatted *Advance Article* as soon as it is available.

You can find more information about *Accepted Manuscripts* in the **Information for Authors**.

NJC

ARTICLE

Effect of pretreatment atmosphere on the activity and selectivity of Co/*meso*HZSM-5 for Fischer-Tropsch Synthesis

Xiaohui Sun,[a] Sina Sartipi,[a] Freek Kapteijn[a] and Jorge Gascon*[a]

The structure and catalytic performance of bifunctional 10 wt.% Co/*meso*HZSM-5 catalysts pretreated under different conditions, *i.e.* in stagnant air, or in a flow of air, N_2, or 1 vol.% NO/Ar, were investigated for the Fischer-Tropsch synthesis (FTS) under fixed operating conditions of T = 513 K, P = 15 bar, H_2/CO = 1. The combination of acid sites and FTS functionality leads to the direct formation of gasoline range hydrocarbons and suppresses the formation of C20+ products. The highest activity, C5-C11 selectivity and lowest CH_4 selectivity were obtained for Co/*meso*HZSM-5 catalyst pretreated in stagnant air. Pretreatment in gas flow resulted in a lower activity and C5-C11 selectivity, and in a higher CH_4 selectivity, in particular for samples pretreated with NO. Characterization shows that this underperformance is due to changes in the Co_3O_4 particle size distribution and cobalt reducibility, and is related to the cobalt loading relative to the mesopore area. Pretreatment in air or N_2 flow increased the number of small Co_3O_4 particles and increased cobalt reducibility by suppressing the formation of highly dispersed cobalt, e.g. cobalt silicates, in strong interaction with *meso*HZSM-5. Pretreatment in a 1 vol.% NO/Ar flow significantly increased cobalt dispersion further, decreasing the cobalt reducibility due to the strong interaction between cobalt and *meso*HZSM-5. Based on both TEM and *in-situ* DRIFTS studies, the optimum performance of Co/*meso*HZSM-5 pretreated in stagnant air could be attributed to a lower fraction of small cobalt particles, known to promote the formation of CH_4 *via* hydrogenolysis or direct methanation. Additionally, small cobalt particles are more susceptible to be oxidized under FT conditions, thereby decreasing FT activity and indirectly increasing CH_4 selectivity by increasing the H_2/CO ratio through the water gas shift reaction.

Introduction

The gradual depletion of crude oil has resulted in the resurrection of Fischer-Tropsch synthesis (FTS) in both industrial and academic research. Fischer-Tropsch synthesis is a feasible route to produce clean liquid fuels such as gasoline and diesel oil free of sulphur and aromatic compounds from syngas (mixture of H_2 and CO obtained from natural gas, coal or biomass) [1-3]. In spite of recent promising results with iron based catalysts [2-4], supported cobalt is the preferred catalyst for FTS because of its low water-gas-shift (WGS) activity, relatively low price compared to ruthenium, and high activity and selectivity towards long chain hydrocarbons [5, 6]. In this sense, the traditional Fischer-Tropsch synthesis is always followed by product upgrading units in which hydrocracking and/or isomerization of FTS products is carried out. One way to achieve the intensification of the abovementioned process is by combining the FTS functionality with the acidity of zeolites [7-11].

The combination of an FTS active phase with zeolites which could "break" the classical Anderson-Schulz-Flory (ASF) product distribution can be traced back to 1980s [12]. However,

methane selectivity in these bifunctional FT catalysts reached as high as 20%, in spite of a higher selectivity towards hydrocarbons in C5-C11 fractions and lower C12+ selectivity compared to the conventional Co-based catalysts [7, 13-15]. Recently, the introduction of mesoporous structures in Co/HZSM-5 system has been proven to effectively decrease methane selectivity and further increase C5-C11 selectivity in comparison with Co/HZSM-5, attributable to both the reduced diffusion path-length and resistance for reactants and/or products [16] and the decrease of acidity in mesopores [7, 13-16]. However, CH_4 selectivity is still twice as high as that in Co/SiO_2 with the same Co content [7, 13-15]. By transmission electron microscopy, Sartipi *et al.* [14] showed that Co particles are inhomogeneously distributed over Co/*meso*HZSM-5, with a large percentage of these particles being smaller than 6 nm, even at moderately high 20 wt.% cobalt loadings.

Generally speaking, FT reaction is structure sensitive, with methane selectivity increasing as cobalt particle size decreases below 8-10 nm [17-21]. Small cobalt particles with a large fraction of edge/corner sites participate in the direct hydrogenation of CH_x species to methane, thereby giving rise to high CH_4 selectivity [17, 18]. At the same time, the FTS activity of Co-based catalysts, expressed by the cobalt-time yield (*CTY*), is related to the number of cobalt atoms on the surface, therefore depends on the cobalt particle size and exhibits a volcano-like curve with the optimum cobalt particle size at around 6-10 nm [17, 19-

[a.] Catalysis Engineering, Department of Chemical Engineering, Delft University of Technology, Julianalaan 136, 2628 BL Delft, The Netherlands. E-mail: J.Gascon@tudelft.nl; Fax: +31 15 27 89820.

ARTICLE

[21]. Thus, the search for methods to optimize the cobalt particle size and dispersion has triggered intense investigations by a number of research groups [22-25].

Martínez *et. al* [23] showed that cobalt dispersion over SBA-15 was improved by changing cobalt precursors from nitrate to acetate and acetylacetonate. Such an improved dispersion resulted in a lower reducibility and activity and in higher CH_4 selectivity. Addition of rhenium [6, 26] promoted the activity of 20 wt.% Co/SBA-15 and decreased CH_4 selectivity, which was assigned to the higher reducibility and to the more uniform dispersion of cobalt species in this sample [23]. However, the introduction of 0.3 wt.% ruthenium in 20 wt.% Co/*meso*HZSM-5 neither changed methane selectivity nor catalytic activity [14].

Recent research [27-34] by De Jong and co-workers showed that the activity of supported metal nanoparticles could be remarkably influenced by various factors during catalyst pretreatment, including temperature [27, 31], atmosphere [28-30, 33, 34], and gas-hourly-space-velocity (*GHSV*) [31, 32]. Co-based FT catalysts (-SiO$_2$, -Al$_2$O$_3$) had a maximum cobalt-time yield (*CTY*) activity, in spite of a slightly increased CH_4 selectivity, after fluid-bed drying at 100 °C in an appropriate N_2 flow. This was attributed to the improved cobalt dispersion by preventing formation of large cobalt aggregates, thereby enlarging the spacing between cobalt crystallites [27, 31]. When the gas atmosphere was varied from inert to air, large particles were observed [31]. In contrast, highly dispersed Co_3O_4 particles with dimensions around 4-5 nm were formed in 18 wt.% Co/SiO$_2$ catalysts by using a 1 vol.% NO/He flow [19, 30]. These highly dispersed cobalt nanoparticles exhibited excellent *CTY* activities in FTS, although no methane selectivities were presented. Similar results were also published by Wang *et al.* [9] by changing Co/SiO$_2$ to Co/HZSM-5. They showed that using a gas flow during catalyst pretreatment improved the FT activity, and 8 wt.% Co/HZSM-5 pretreated in a 5 vol.% NO/Ar flow exhibited much higher CO conversion than after calcination in air.

Recent studies [7, 13] in our group have shown that formation of mesopores in the zeolite support resulted in an improved activity and stability, and in a lower CH_4 selectivity than for Co/HZSM-5 catalysts. In this work, we further extend our study by focusing on fine-tuning Co dispersion by varying catalyst pretreatment conditions. Structural properties and catalytic performance of the resulting catalysts is evaluated by combining detailed characterization and catalytic testing.

Experimental

Materials

ZSM-5 zeolite (Si/Al = 40) in ammonium form was purchased from Zeolyst (CBV 8014). TPAOH (1 M), HNO$_3$ (70 wt.%), Co(NO$_3$)$_2$·6H$_2$O (> 99%) were purchased from Sigma-Aldrich. All chemicals were used without any further purification.

Support preparation and catalyst synthesis

ZSM-5 in ammonium form was calcined at 823 K for 5 h to obtain HZSM-5. Mesoporous HZSM-5 was synthesized by base and acid treatment, as reported previously [14]. Desilication was carried out in 1 M TPAOH aqueous solution (volume$_{base solution}$/mass$_{zeolite}$ = 8.0 cm^3/g) in a capped bottle with continuous stirring at 343 K for 1 h in an oil bath. This bottle was then immediately cooled in ice to terminate the reaction. After desilication the zeolite powders were centrifuged and washed to neutral pH with deionized water, followed by drying at 393 K for 12 h and calcined at 823 K for 5 h. The obtained samples were then treated in 1 M HNO$_3$ aqueous solution (volume$_{acid solution}$/mass$_{zeolite}$ = 28.6 cm^3/g) at 343 K for 2 h under stirring in the same oil bath. Then the samples were quenched, washed, dried, and calcined the same as for desilication. The acid treated zeolite is denoted as *meso*HZSM-5.

Catalysts were prepared by incipient wetness impregnation (IWI) of *meso*HZSM-5 (38-75 μm) with an aqueous solution of Co(NO$_3$)$_2$·6H$_2$O to reach a nominal 10 wt.% Co loading. The impregnated samples were kept in a desiccator at room temperature overnight, followed by drying in a reactor (ID = 2 cm) in upflow mode with air, N_2 or 1 vol.% NO/Ar at a *GHSV* of 4500 h^{-1} at 373 K for 12 h (2 K/min) and then further heating to 623 K for 1 h (1 K/min) in the same atmosphere. Another impregnated sample was dried in an oven in a crucible (ID = 7.5 cm) at 373 K for 12 h (2 K/min) and then further heated to 623 K for 1 h (1 K/min) in stagnant air. The amount of the impregnated samples used during the pretreatment step is based on 0.5 g *meso*HZSM-5 support. Notation of the catalysts corresponds with the pretreatment atmosphere used (-stag, -air, -N_2, or -NO).

Characterization

N_2 physisorption was measured by Micromeritics Tristar 3020 apparatus at 77 K after degassing under vacuum overnight at 623 K in Micromeritics Vacprep 061 apparatus. In each experiment 100 mg sample was used. Pore size distribution was obtained by the density functional theory (DFT) method assuming a slit pore geometry (slit pore-N_2 DFT model) [35].

Chemical analysis was performed by inductively coupled plasma optical emission spectrometry (ICP-OES) in Perkin-Elmer Optima instruments. Appropriately 25 mg of each sample was dissolved in a mixture of 4 ml 30% HCl, 1 ml 65% HNO$_3$ and 1 ml 40% HF with a microwave oven (900 W; hold for 15 min). The solutions were diluted in a ratio of 1:10 in milli-Q water and then the analysis was performed.

X-ray diffraction (XRD) patterns were recorded in Bragg-Brentano geometry in Bruker D8 Advance X-ray diffractometer equipped with a Vantec position sensitive detector and graphite monochromator. Measurements were performed at room temperature with monochromatic Co *K*☒ radiation (*λ* = 0.179026 nm) in the 2Θ range (5° - 90°). The samples were placed on a Si (5 1 0) substrate and rotated during measurements. The average particle sizes of Co_3O_4 in these catalysts were calculated from Scherrer equation using the most intense reflexion at 2Θ = 43.07°, and the average cobalt particle size was calculated with the following relation [36]:

$$d(Co^0) = 0.75 \times d(Co_3O_4) \tag{1}$$

Transmission electron microscopy (TEM) analysis was performed by using an electronic microscope (JEOL JEM-2010) operating at a voltage of 200 kV. The freshly prepared sample powder was ultrasonically dispersed in ethanol and deposited on a copper grid prior to the measurement.

Temperature-programmed reduction in hydrogen (TPR(H_2)) was performed in a homemade equipment with a packed bed of 100 mg of fresh catalyst (100-212 µm) in a flow of 10 vol.% H_2/Ar (30 ml/min) at a heating rate of 5 K/min. The reactor temperature was increased from ambient temperature to 1273 K and after water removal, the H_2 consumption ($n(H_2)_{total}$) was monitored by a TCD calibrated with CuO.

The reactor temperature was ramped from room temperature to 673 K (5 K/min) and stayed there for 5 h in a flow of 10 vol.% H_2/Ar (30 ml/min), followed by cooling down to 473 K. After the signal had become stable, the reactor temperature was heated to 1273 K (5 K/min) and H_2 consumption ($n(H_2)_{>673K}$) was measured. The consumption of H_2 below 673 K is calculated as follows,

$$n(H_2)_{<673\,K} = n(H_2)_{total} - n(H_2)_{>673\,K} \qquad (2)$$

Then the extent of Co reduction was calculated from the amount of H_2 consumed below 673 K needed for a complete reduction of a fraction of the assumed Co_3O_4 starting compound to Co^0 during the in-situ reduction treatment at 673 K.

In situ DRIFTS of CO adsorption was performed in a Nicolet 6700 FT-IR (Thermo Scientific) equipped with a MCD/A detector in order to characterize the cobalt species in Co/*meso*HZSM-5 catalysts [13]. Samples were reduced by pure H_2 flow (20 cm^3_{STP}/min) at 673 K for 4 h (5 K/min). Afterwards, the cell was evacuated with He at 673 K for 30 min to remove the adsorbed H_2 molecules on the cobalt surface, followed by cooling down to 303 K under He flow (20 cm^3_{STP}/min). Then 1.5 vol.% CO/He (30 cm^3_{STP}/min) was fed to the cell for 30 min at 303 K. Subsequently, the catalysts were flushed in He (20 cm^3_{STP}/min) for 1 h. Then the IR spectra were consecutively collected at 473 K and 513 K. Spectra of KBr at 303 K were recorded as background, and sample spectra collected at 573 K after total CO desorption under He flow (20 cm^3_{STP}/min) were used as reference.

Catalyst performance

FTS experiments were performed in a six-flow fixed-bed microreactor (FBM) setup as previously described [37, 38]. 0.5 g fresh catalysts (100-212 µm) was mixed with SiC of similar size to keep a constant fixed bed volume of 1.3 cm^3. Prior to the FTS operation, catalysts were activated *in-situ* by H_2 (80 cm^3_{STP}/min) at 673 K for 10 h at atmospheric pressure, followed by cooling to 453 K. As the pressure was increased to 15 bar (FT operation), CO was gradually introduced in the feed stream at 453 K until reaching a final H_2/CO ratio of 1. Then the reactor was heated to the reaction temperature of 513 K to reach the used standard operating conditions with a gas-hourly space velocity (*GHSV*) of 6 m^3_{STP} kg_{cat}^{-1} h^{-1}. All the heating and cooling steps were performed at 2 K/min. Waxes were collected by gas/liquid separators at 448 K and 15

bar during FTS experiments. Liquid hydrocarbons and water were collected in cold traps at 278 K at atmospheric pressure. These liquid hydrocarbons and waxes were weighed and dissolved in CS_2 separately. Then these samples were analysed offline by a simulated distillation (SimDis) GC (Hewlett Packard 5890, Series II) equipped with an FID and HP-1 column (7.5 m × 0.53 mm, film thickness 2.65 µm), with a carrier gas of He. The oven temperature in the analysis was programmed from 308 K to 623 K (14 K/min) and kept at the final temperature for 5 min.

Permanent gases as well as light hydrocarbons in the gas phase were analyzed online by a Compact GC (Interscience) equipped with three columns and detectors in parallel using He as carrier gas. In the first column (Carboxen 1010, 10 m × 0.32 mm) N_2, CO, CH_4 and CO_2 were separated at 333 K and analyzed by TCD. In the second column (Al_2O_3/KCl, 10 m × 0.32 mm) and FID detection, separation between all C1–C4 components was achieved at 434 K. In the third column (RTx-1 0.5µm, 15 m × 0.32 mm) C5–C10 hydrocarbons were separated at 353 K and analyzed by FID.

The selectivity was determined after 92.5 h when a pseudo-steady-state was reached. CO conversion and carbon selectivity were defined as follows,

$$X_{CO} = \frac{F_{in,CO} - F_{out,CO}}{F_{in,CO}} \times 100\% \qquad (3)$$

$$S_{C_n} = \frac{nF_{C_n}}{F_{CO_2} + \sum_{n=1}^{N} nF_{C_n}} \qquad (4)$$

where X_{CO} stands for CO conversion, *F* indicates the molar flow rate, S_{C_n} is the carbon selectivity towards a product with *n* carbon atoms.

Results

Bifunctional Co/*meso*HZMS-5 catalysts were prepared using incipient wetness impregnation (IWI), followed by pretreatment under different gas conditions. The structural and catalytic properties of these Co/*meso*HZSM-5 catalysts will be discussed below in detail.

Structural characterization

N₂ adsorption and X-ray diffraction

Table 1 Textual properties obtained from N_2 adsorption isotherms at 77 K and cobalt loading of mesoHZSM-5 supported Co catalysts

Samples	S / (m²/g)		V / (cm³/g)ᶜ			Co wt.%ᵍ
	Totalᵃ	Mesoᵇ	wt.%ᵍ	Microᵉ	Mesoᶠ	
*meso*HZSM-5	717	491	0.62	0.1	0.52	-
Co/*meso*HZSM-5						
-stag	591	374	0.57	0.1	0.46	10.5
-air	596	379	0.58	0.1	0.47	10.5
-N₂	544	345	0.52	0.1	0.41	9.3
-NO	560	349	0.53	0.1	0.42	8.9

a: BET area based per gram *meso*ZSM-5. b: Mesopore surface area obtained from the *t*-plot applied to the N_2 isotherm. c: Pore volume based per gram *meso*ZSM-5. d: Total pore volume. e: Micropore volume obtained from the *t*-plot. f: Mesopore volume calculated as $V_{meso} = V_{total} - V_{micro}$. g: Obtained from ICP-OES.
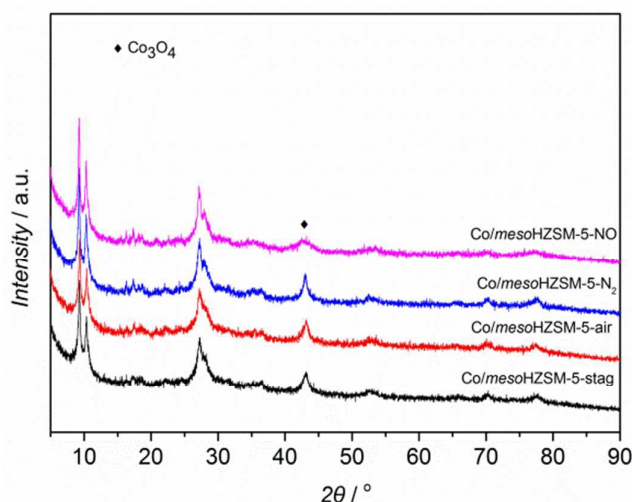
Fig. 1 X-ray diffraction patterns of Co/*meso*HZSM-5 catalysts with different pretreatment conditions

The textural properties of all Co/*meso*HZSM-5 catalysts are shown in Table 1. After cobalt impregnation, the BET area and mesopore volume (based on support mass) of *meso*HZSM-5 in Co/*meso*HZSM-5 catalysts are lower than those of the initial *meso*HZSM-5 (717 m^2/g and 0.62 cm^3/g) support, while mesopore size distribution is similar (Fig. S1, ESI†). The mesopore volumes were different after each pretreatment atmosphere, being smaller when either N_2 or 1 vol.% NO/Ar flows are used. ICP analysis demonstrates that cobalt loadings in all catalysts are close to 10 wt.%, consistent with the targeted value.

The XRD patterns of all freshly prepared Co/*meso*HZSM-5 catalysts are shown in Fig. 1. The reflections characteristic for the MFI structure of HZSM-5 can be observed, indicating the crystalline structure present after the consecutive base and acid treatment [39]. Further, only Co_3O_4 reflections can be identified [7, 13, 14], indicative of the decomposition of cobalt nitrate after the pretreatment. Line-broadening analysis (Table 2) shows that Co/*meso*HZSM-5 catalysts pretreated in stagnant air or air flow result in Co_3O_4 crystallites of 12 nm on average, while the average Co_3O_4 crystal size increases to 17 nm after treatment in a pure N_2 flow as shown by the narrower and more intense diffraction peak in Fig. 1. Adding 1 vol.% NO to Ar flow results in the formation of Co_3O_4 crystallites of 9 nm on average, characterized by the low and broad reflection (Fig. 1). The observed differences indicate that the pretreatment atmosphere has an impact on the size and distribution of cobalt species, in agreement with other reports [32, 34].

Transmission electron microscopy (TEM)

Freshly prepared Co/*meso*HZSM-5 samples were studied by TEM, as shown in Fig. 2. All catalysts exhibit a spongy morphology, representative of the mesoporous support [13]. Large Co_3O_4 aggregates can be observed in Co/*meso*HZSM-5-stag sample (Fig. 2a, e), which are composed of small Co_3O_4 crystals smaller than 15 nm, consistent with the mean particle
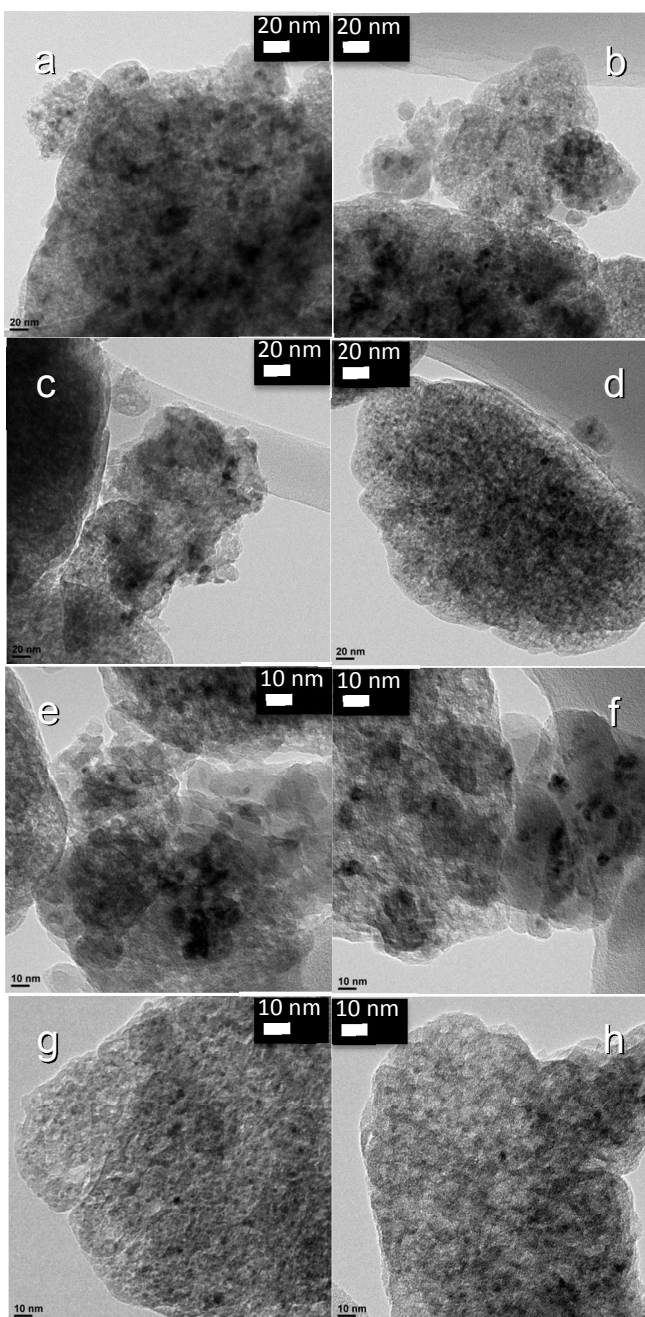
Fig. 2 TEM images for Co/*meso*HZSM-5 with different pretreatment conditions: (a,e) Co/*meso*HZSM-5-stag, (b,f) Co/*meso*HZSM-5-air, (c,g) Co/*meso*HZSM-5-N_2, (d,h) Co/*meso*HZSM-5-NO.

size (12 nm) estimated by XRD. Co_3O_4 particles could hardly be detected on the outside of the support, indicating that most Co species are inside the mesopores [14]. Pretreatment in a gas flow does not only impact the Co_3O_4 particle size but also the particle size distribution. An almost bimodal particle size distribution is found in the air-flow pretreated sample, with smaller Co_3O_4 particles (Fig. 2b) than for the '-stag' one, and some larger ones at the external part of the support. This scenario is more pronounced in the '-N_2' sample where a few
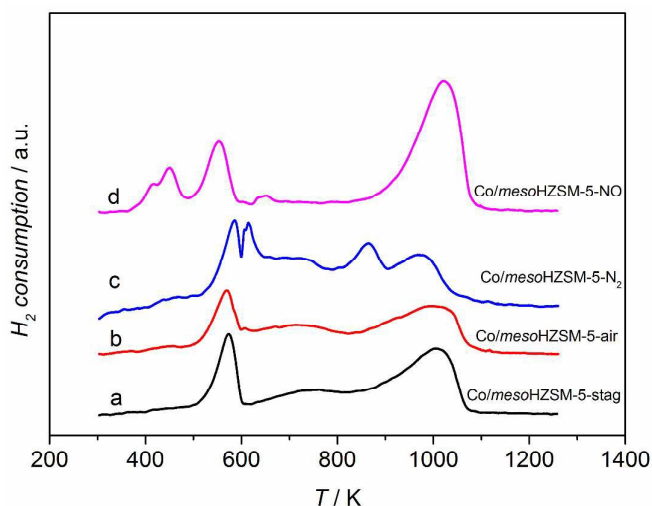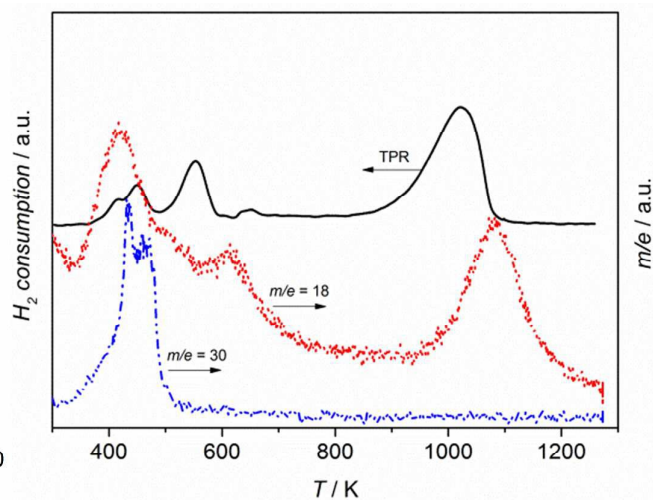
Fig. 3 TPR(H_2) profiles (5 K/min) of Co/*meso*HZSM-5 catalysts prepared under different gas conditions. H_2 consumption normalized for the Co content of the samples

Fig. 4 Products analysis of Co/*meso*HZSM-5-NO catalyst in TPR(H_2) profile

Co_3O_4 particles larger than 30 nm (Fig. S2, ESI†) together with a highly dispersed Co_3O_4 phase (Fig. 2g) are observed, in agreement with the more intense XRD diffraction lines, dominated by the large particles. Large nanoparticles (CuO or NiO) were also observed on the external surface of the support (SiO_2 [32] or SBA-15 [34]) when catalysts were prepared at a low space velocity. Finally, in the Co/*meso*HZSM-5-NO sample, a large number of well-distributed Co_3O_4 nanoparticles is found with crystallite sizes not larger than 8 nm (Fig. 2d, h).

Reducibility of cobalt species in Co/*meso*HZSM-5 catalysts

Fig. 3 shows the TPR(H_2) profiles for all Co/*meso*HZSM-5 catalysts. The TPR profiles have been normalized by per mass of cobalt in the catalysts. The multiple reduction peaks in Co/*meso*HZSM-5 stand for heterogeneity of reducible cobalt species and several cobalt reduction steps [40, 41].
In good agreement with previous studies [14], Co/*meso*HZSM-5-stag exhibits a sharp reduction peak at approximately 575 K, followed by a broad reduction band ranging from 600 K to 900 K, and a peak above 900 K. The '575 K' peak can be assigned to the reduction of Co^{3+} to Co^{2+} and some Co^{2+} to Co^0 [13, 22, 42], which weakly interacts with *meso*HZSM-5. Note that the reduction temperature of CoO particles is related to the interaction between cobalt species and the support [23], the broad feature thus illustrates the stabilisation of CoO in different interaction with *meso*HZSM-5, representative of the heterogeneous distribution in particle sizes [40, 43]. The peak above 900 K has been ascribed to the reduction of highly dispersed cobalt oxide in strong interaction with *meso*HZSM-5 [22, 40]. TPR profiles of Co/*meso*HZSM-5 depend on the pretreatment atmosphere. The peak area above 900 K, corresponding to hardly reducible Co species decreases, and the broad feature increases for the '-air' and '-N$_2$' sample, particularly for the latter. Besides, a doublet below 650 K can be observed in Co/*meso*HZSM-5-N$_2$ sample, indicative of
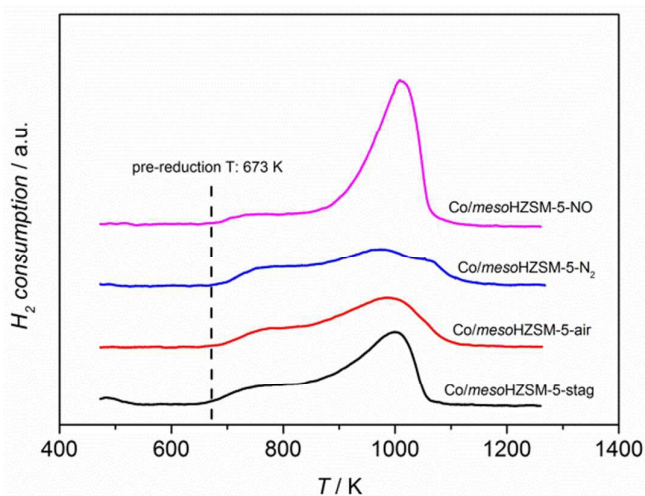
Fig. 5 TPR(H_2) profiles (5 K/min) of pre-reduced Co/*meso*HZSM-5 catalysts at 673 K for 5 h. H_2 consumption normalized for the Co content of the samples

big Co_3O_4 particles [41], as confirmed by XRD and TEM results.
The TPR profile of Co/*meso*HZSM-5-NO contains a doublet below 500 K. The reduction products were analysed using a mass spectrometer, and the results are shown in Fig. 4. A signal at m/e = 30 accompanied by the formation of water is observed at around the temperature of the low-temperature reduction peak, confirming a reduction process. The m/e = 30 value stems from the NO^+ ion, which is the most intense fragment contribution of both NO and NO_2 [43]. Accordingly, the low-temperature peak can be assigned to the reduction of residual cobalt nitrate present after the thermal treatment. Additionally, the sharp reduction peak appears 25 K below the temperature observed for the other catalysts, tentatively attributed to the reduction promoted by hydrogen spillover from the Co reduced below 500 K. The broad feature

disappears while the peak area above 900 K significantly increases, indicating the existence of a large fraction of hardly reducible cobalt species.
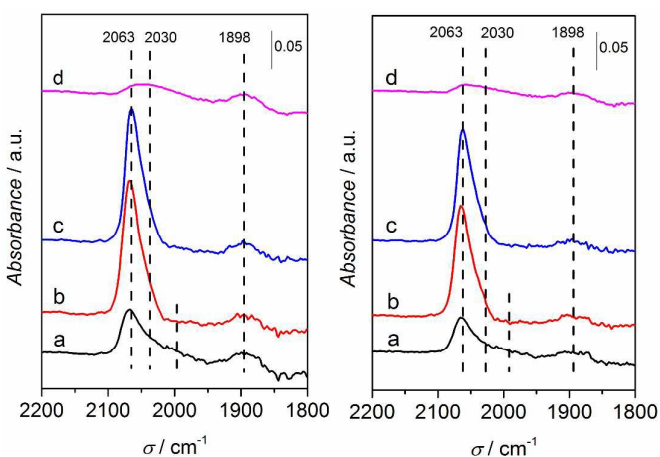
In order to determine the cobalt reducibility, all catalysts were pre-reduced at 673 K for 5 h, corresponding to the pretreatment before the FTS operation, and a TPR profile was recorded afterwards (Fig. 5). The appearance of several broad reduction peaks above 673 K after 'pre-reduction' proves the presence of poorly reducible Co species under the applied FTS activation temperature, as shown in Table 2.

In situ CO-FTIR characterization of Co/*meso*HZSM-5 catalysts

FTIR spectroscopy of adsorbed CO has been widely employed to investigate the nature of surface sites in most transition metal catalysts, due to the sensitivity of the CO stretching frequency to the electronic state of the adsorption sites [42, 44].

Figure 6 shows the results obtained applying this technique on the different Co/*meso*HZSM-5 at 473 K and 513 K. Earlier research from our group confirmed that CO desorbed completely at 473 K from the zeolite surface [13], eliminating the interference from adsorption on acid sites in the spectra. Two regions, 2100-2000 cm^{-1} and 1850-1950 cm^{-1} are observed in the spectra of pre-adsorbed CO over all these Co-based catalysts, ascribable to linear and bridged adsorption of CO, respectively, on metallic cobalt sites [44, 45]. The exact identification of the 2063 cm^{-1} band is still controversial in the literature, where this band has been often ascribed to different species: (i) $Co(CO)_n$ ($n>1$) species attached to cobalt defect sites [46, 47], (ii) a blue shift of the intensity maximum at high coverage of linearly adsorbed CO due to long range dipole-dipole interactions [46], (iii) a structure of hydrocarbonyl [48] and (iv) CO adsorbing on $Co^{\delta+}$ sites [47-49]. The assignment to $Co(CO)_n$ ($n>1$) and the dipole-dipole interactions can be excluded in our results as this band does not shift to lower wavenumber after increasing temperature to 513 K, although the band intensity decreases due to some CO desorption from cobalt sites at higher temperature. Additionally, the attribution of the 2063 cm^{-1} band to hydrocarbonyl species is neither appropriate because hydrocarbonyl is unstable and only present in the presence of co-adsorbed hydrogen [50], which is not the case in the experiments here reported (samples were flushed in He at 673 K prior to CO adsorption). Thus the 2063 cm^{-1} band can be ascribed to CO species adsorbed on Co^0 sites with weak electron-donor properties (with partial positive charge $Co^{\delta+}$) [49, 51] in close contact with *meso*HZSM-5 or unreducible cobalt oxides, since these partially oxidized species result in a certain electropositive character of the Co ($Co^{\delta+}$) [44]. The amount of these cobalt sites ($Co^{\delta+}$) significantly increases when comparing samples pretreated in stagnant air and samples activated in air- and N_2 flow, with a much larger contribution of these sites in the latter cases. In contrast, the relative intensity of this band in Co/*meso*HZSM-5-NO decreases strongly. The 2063 cm^{-1} band with a contribution at a lower wavenumber (ca. 2030 cm^{-1}), especially for '-stag' sample, has been attributed to CO molecules linearly bonded on surface cobalt atoms of relatively large metal particles [48, 51].

Table 2 Physico-chemical properties of cobalt phases in Co/*meso*HZSM-5 catalysts as determined from XRD and TPR(H_2) characterization

| sample	XRD		Extent of Co reduction (%)
	Co_3O_4 diameter (nm)	Co diameter (nm)	
Co/*meso*HZSM-5			
-stag	12	9	28
-air	12	9	34
-N$_2$	17	13	45
-NO	9	7	-

Fig. 6 DRIFT spectra of CO adsorbed on Co/*meso*HZSM-5 (*left*: 473 K, *right*: 513 K) with different pretreatment conditions: (a) Co/*meso*HZSM-5-stag, (b) Co/*meso*HZSM-5-air, (c) Co/*meso*HZSM-5-N₂, (d) Co/*meso*HZSM-5-NO.
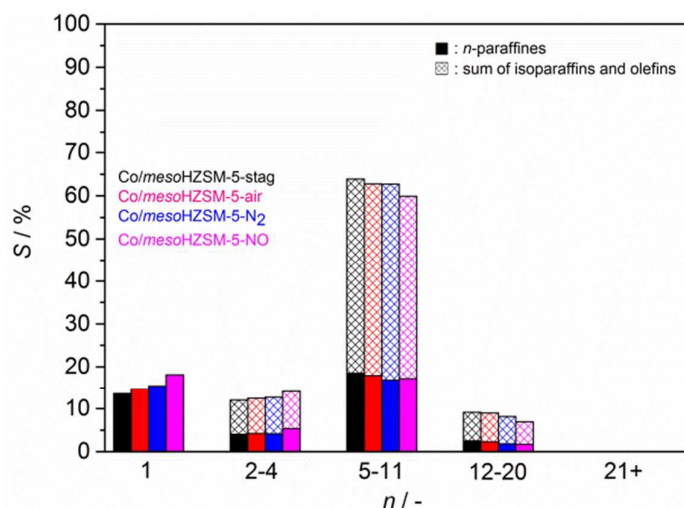
Furthermore, the '-stag' sample also contains a tail ranging from 2010 cm^{-1} to 1995 cm^{-1}, indicating the heterogeneity of cobalt adsorption sites [52], in good agreement with the inhomogeneous particle-size distribution observed by TEM.

The intensity of the band around 1898 cm^{-1} which is ascribed to bridged adsorbed CO on relatively large cobalt particles [44] also decreases after changing pretreatment atmosphere from stagnant air to gas flows, indicating a decrease in the amount of large cobalt particles in the latter cases.

Catalytic performance in FTS

Time-on-stream (*TOS*) evolution of CO conversion over all these Co/*meso*HZSM-5 samples is presented in Fig. 7. As a function of *TOS*, all tested catalysts display similar behaviour, with a gradual deactivation before reaching 'steady state' after approximately 50 h on stream. Co/*meso*HZSM-5 catalysts pretreated under different atmospheres exhibit different CO conversion levels, which is consistent with the general belief that Co-based FT catalysts are structure sensitive [17-19]. The '-stag' sample shows the highest CO conversion (36%) and cobalt-time yield (*CTY*) (0.46 mol_{CO} g^{-1}_{Co} h^{-1}) in comparison with samples pretreated in gas flows (Table 3) after 92.5 h. This is
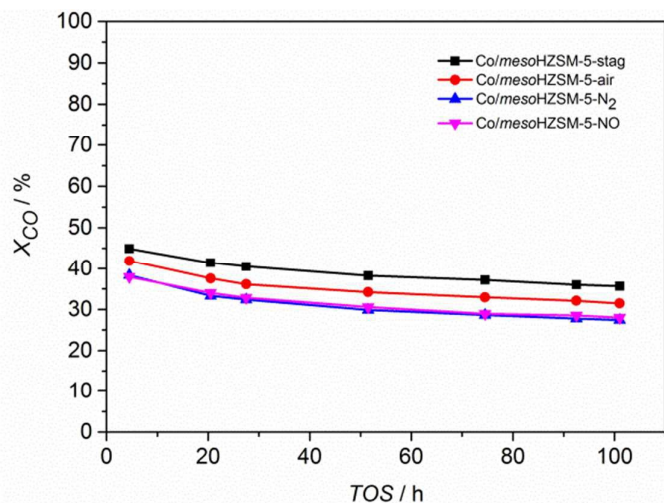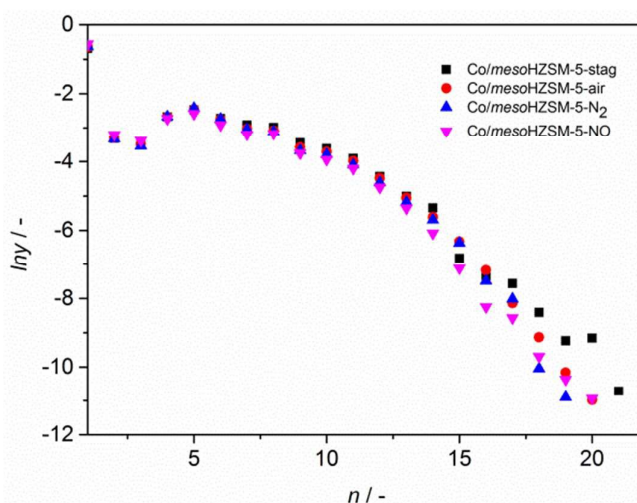
Fig. 7 Time-on-stream (*TOS*) evolution of CO conversion for Co/*meso*HZSM-5 prepared in different ways during FTS at 513 K, 15 bar total pressure, feed composition $H_2/CO = 1$, and *GHSV* = 6 m^3_{STP} kg^{-1}_{cat} h^{-1}.

Fig. 9 ASF plot after 92.5 h on-stream at 513 K, 15 bar total pressure, $H_2/CO = 1$, and *GHSV*= 6 m^3_{STP} kg^{-1}_{cat} h^{-1}.
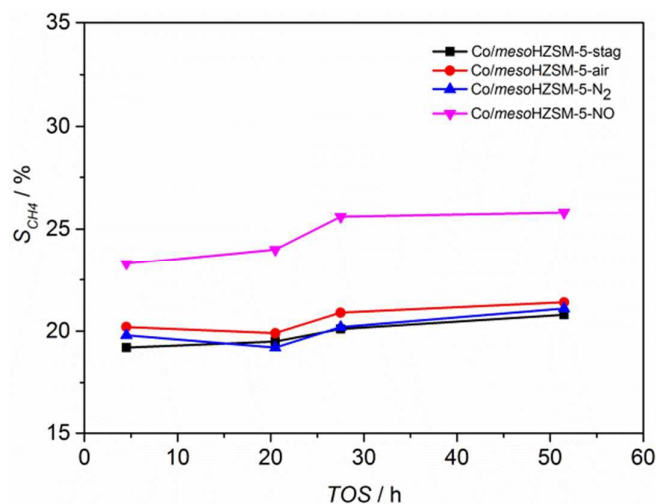

Fig. 8 Carbon selectivity toward products of FTS after 92.5 h on stream. In each group from left to right: Co/*meso*HZSM-5-stag, Co/*meso*HZSM-5-air, Co/*meso*HZSM-5-N₂, and Co/*meso*HZSM-5-NO. Experiments were performed at 513 K, 15 bar total pressure, feed composition $H_2/CO = 1$, and *GHSV* = 6 m^3_{STP} kg^{-1}_{cat} h^{-1}. Key: *solid fill n*-paraffins, *hatched fill* olefins and isoparaffins.

Fig. 10 Time-on-stream (*TOS*) evolution of CH₄ selectivity obtained from online GC product for Co/*meso*HZSM-5 prepared in different ways during FTS at 513 K, 15 bar total pressure, feed composition $H_2/CO = 1$, and *GHSV* = 6 m^3_{STP} kg^{-1}_{cat} h^{-1}.

different from Co/SiO₂ [19, 30] and Co/HZSM-5 [9] systems, in which the *CTY* activity for the sample pretreated under NO flow was twice as high as that calcined in air.

The hydrocarbon product distributions for all Co/*meso*HZSM-5 catalysts after 92.5 h are included in both Fig. 8 and Table 3. Carbon balances for these experiments are in every case above 95%. Carbon selectivity to CH₄ and hydrocarbons in C5-C11 fraction is much higher than for Co/SiO₂ catalysts [7, 13, 14], while

that of C12-C20 decreases considerably and no hydrocarbons with carbon chain number larger than 20 were detected. Molar product distributions over these Co/*meso*HZSM-5 after 92.5 h on stream are presented in Fig. 9. Unlike Co/SiO₂ FT catalysts, for which the molar product distributions *versus* their carbon number follows a linear trend [13], Co/*meso*HZSM-5 catalysts prepared in our experiments exhibit a break in the ASF distribution at around C12 and molar fractions of hydrocarbons drop remarkably as their carbon number exceeds the upper limit of gasoline range, due to the hydrocracking over the acid sites [7, 13-15]. The trend in CH₄ selectivity for different catalysts follows the order of

ARTICLE

Table 3 CO conversion, chain growth probability factor (α), C1, C5-C11, C5+, and CO_2 carbon selectivities of FTS products after 92.5 h for Co/*meso*HZSM-5 synthesized in different ways.

Sample	X_{CO} [a] (%)	CTY [b]	S [%]				$α$ [c]
			C1	C5-C11	C12+	CO2	
Co/*meso*HZSM-5							
-stag	36.0	0.46	13.5	63.8	10.2	1.4	0.79
-air	32.1	0.41	14.8	62.7	9.0	1.1	0.78
-N₂	27.8	0.40	15.5	62.7	8.1	1.0	0.76
-NO	28.5	0.43	18.1	59.9	6.9	1.0	0.76

Reaction conditions: T = 513 K, P = 15 bar, H2/CO = 1, $GHSV$ = 6 m$^3_{STP}$ kg$^{-1}_{cat}$ h^{-1}. a: The maximum deviation from the average conversion value (between FBM 1-6) is ± 2% [37]. b: cobalt-time-yield: mol $_{CO}$ g$^{-1}_{Co}$ h^{-1}, c: chain growth probability ($α$) obtained from the ASF plot in the C5–C11 hydrocarbon range.

Co/*meso*HZSM-5-stag < Co/*meso*HZSM-5-air < Co/*meso*HZSM-5-N₂ < Co/*meso*HZSM-5-NO, while selectivities to the C5-C11 and C12-C20 product ranges decrease in this order (Fig. 8). The increased selectivity to longer-chain hydrocarbons concurs with the increase in cobalt particle and aggregate size (Fig. 2), in agreement with earlier reports where C5+ selectivity relates to sizes of cobalt particles above 8 nm [17]. Also, large aggregates were reported to increase selectivity to long chain alkanes, probably due to the re-adsorption and secondary chain growth of olefins [27, 31], by which the chain growth probability factor ($α$) may be larger. For all samples the CO_2 selectivity is below 2%, revealing a relatively low water-gas-shift (WGS) activity for Co-based catalysts under this reaction condition.

Finally, in order to check how CH₄ selectivity behaves in the initial reaction period, CH₄ selectivity *versus TOS* is displayed in Fig. 10. Note that to arrive to these plots a constant production of liquid hydrocarbons over *TOS* was assumed, since only gas products can be analyzed online. The CH₄ selectivity increases with *TOS*, in agreement with previous results [14], attributed to a combination of the partial oxidation of small Co aggregates with *TOS*, and the higher hydrogen partial pressure level due to the lower CO conversion.

Discussion

The results show that catalytic performance of Co/*meso*HZSM-5 catalysts strongly depends on the pretreatment atmosphere after impregnation. The introduction of a gas flow during this pretreatment step changes the Co_3O_4 particle size distribution and cobalt reducibility compared to Co/*meso*HZSM-5 prepared in stagnant air, in which Co_3O_4 particles distribute inhomogeneously, with scattered large aggregates.

Influence of pretreatment conditions on cobalt particle distribution

Previous research [27, 31] has shown that the size and distribution of supported nanoparticles are influenced by both the support and the pretreatment conditions. Munnik et al. [27] investigated extensively the difference in cobalt dispersion with γ-Al₂O₃ and SiO₂ supported cobalt catalysts. Higher cobalt dispersion was

obtained on γ-Al₂O₃ support, and this was attributed to the increased precursor-support interactions in comparison with silica. Note that *meso*HZSM-5 prepared under consecutive base and acid treatment exposes a large number of silanol groups [13, 39] on the surface. These silanol groups can act as anchoring sites for Co^{2+} cations of the precursor, increasing the interaction between cobalt species and the surface of the support. The strong interaction between cobalt and *meso*HZSM-5 improves the dispersion of cobalt species on the support and results in many cobalt oxide particles of small size as shown in Fig. 2.

Aggregation of cobalt oxide can be controlled by changing the humidity during the pretreatment, and hence the decomposition of metal hydroxynitrate during the drying and calcination steps [30, 33, 34]. The drying temperature employed in our study (373 K) has been proven to balance the removal rate of water and the precipitation rate of nitrate during the drying step [27, 31].

Oxygen, a decomposition product of metal hydroxynitrate during calcination (stagnant air and air flow), has been reported to promote the sintering or redistribution of metal oxides (NiO or Co_3O_4) [30, 33, 34] and may be the cause of the formation of larger Co_3O_4 aggregates in Co/*meso*HZSM-5-stag catalyst. Using an air flow during the pretreatment step leads to the formation of more homogeneously distributed small cobalt oxide particles in Co/*meso*HZSM-5, consistent with the results from De Jong and co-workers [31, 33]. When an inert flow of N₂ is employed, the oxidizing power of the gas is further reduced and results in highly dispersed small Co_3O_4 particles, although some aggregates and large Co_3O_4 particles can be observed in the Co/*meso*HZSM-5-N₂ sample. At a similar $GSHV$ as the one here reported, a bimodal distribution of metal oxides with large particles on the external surface of the supports were also obtained by Munnik *et al.* [32] and Sietsma *et al.* [34]. Finally, a highly dispersed Co_3O_4 phase with a narrow size distribution (< 8 nm) can be found in NO-pretreated Co/*meso*HZSM-5, which is in agreement with earlier reports [30, 34]. NO moderates the decomposition rate of metal hydroxynitrate and lowers the heat of this reaction by NO₂ formation, thereby making the decomposition thermodynamically feasible at lower temperatures than without NO. Furthermore, NO acts as an oxygen scavenger, inhibiting the formation of O₂ during the decomposition of hydroxynitrate, and therefore preventing sintering and redistribution of the active phase. The presence of a highly dispersed Co_3O_4 phase in N₂- and NO-pretreated samples can be also confirmed from N₂ physisorption results, in which pore volumes of *meso*HZSM-5 for these two samples further decrease probably due to the presence of these smaller and highly dispersed particles inside the mesopores [34]. In contrast to our results, Wang *et al.* [9] reported that an optimal cobalt particle size (around 7.7-10.5 nm) in 8 wt.% Co/*meso*HZSM-5 was obtained after pretreatment in a 5 vol.% NO/Ar flow, and the cobalt particle size decreased from 10.5 nm to 7.7 nm when increasing the mesopore surface area in *meso*HZSM-5. Comparing the mesopore areas in the samples used in this work with that in the samples used by Wang *et al*., shows that

in our work it is at least twice as large. Therefore, it is concluded that the dispersion of Co under similar pretreatment conditions is related to the mesopore surface area available for deposition [53] and the targeted cobalt loading. So, depending on the mesopore surface area an optimal pretreatment atmosphere should be selected for a certain Co-loading.

Influence of pretreatment conditions on cobalt particle reducibility

TPR shows that cobalt reducibility (673 K for 5 h) increases after pretreatment from 28% in stagnant air to 34% in airflow and 45% in N_2 flow. TEM results show that more small cobalt oxide particles are present in air- and N_2-pretreated samples (Fig. 2b, g) compared to the '-stag' sample. As mentioned above, the strong interaction between cobalt species and *meso*HZSM-5 leads to the formation of highly dispersed cobalt oxides or even cobalt silicates, which can only be reduced at extremely high temperature (>900 K Fig. 3a). The gas flow (air and/or N_2) inhibits the redistribution of cobalt species and makes the deposition of cobalt hydroxynitrate more homogeneous [30, 31], resulting in well-distributed small cobalt species. These small cobalt oxide particles become easier to be reduced, due to a weaker interaction with the support and a lower surface energy [17, 18, 54], as confirmed by the decreasing reduction peak area above 900 K in Fig. 3b and c. The higher cobalt reducibility of the N_2-pretreated sample compared to '-air' sample can be ascribed to the presence of large Co_3O_4 particles, as confirmed by TEM. However, Co/*meso*HZSM-5 pretreated in 1 vol.% NO/Ar flow shows a significantly large reduction peak area above 900 K. Indeed, as discussed above, the introduction of NO flow during catalysts pretreatment suppresses the sintering and redistribution of cobalt species (cobalt oxides and hydroxynitrate), causing the formation of a highly dispersed cobalt oxide. These highly dispersed cobalt oxides display a very strong interaction with the surface of *meso*HZSM-5. Because the Co/*meso*HZSM-5-NO sample still contains some cobalt nitrate, the cobalt reducibility of this sample would be overestimated from the TPR results (Fig. 3). However, if the cobalt loading and the reduction peaks above 673 K of all catalysts are considered, the NO-pretreated sample shows the largest degree of reduction (Fig. 5). Therefore it is concluded that NO pretreatment decreases the reducibility of cobalt species under the applied FT activation conditions (673 K).

Influence of pretreatment conditions on activity and products selectivity for Co/*meso*HZMS-5 catalysts

FT synthesis occurs on the surface of metallic cobalt particles [17, 18]. The number of active sites is a function of the cobalt particle size, determined by cobalt dispersion and reducibility. Further, the FT reaction is structure sensitive: cobalt particles below 8-10 nm [17-21, 55] are hardly active in FT and produce mostly methane. This is attributed to three effects. Firstly, as cobalt particle size decreases, the amount of coordinatively unsaturated cobalt sites increases, on which CO molecules bind strongly and irreversibly. Such strong adsorption [18]

prevents the insertion of additional CO molecules, promoting the direct hydrogenation of CO to CH_4 [17, 18]. Secondly, small cobalt particles (< 4 nm) are more susceptible to get oxidized at a high p_{H2O}/p_{H2} ratios than larger particles, as proven by both high pressure FT testing [5] and thermodynamic calculations [54]. It goes without saying that oxidized cobalt is not active in FTS. Nevertheless, these oxidized cobalt oxides catalyse the water-gas-shift (WGS) reaction [8, 56-58], which contributes to a higher H_2 to CO ratio. This additional hydrogen promotes the termination step in FTS, decreasing chain growth probability and indirectly increasing overall CH_4 selectivity. Finally, hydrogenolysis [8, 14, 59] is known to occur during FT reaction by which extra CH_4 can be produced.

Mesoporous zeolite based FT catalysts [7, 9-11, 13-16] are very interesting systems because of their high activity, C5-C11 selectivity and lower C20+ selectivity compared to conventional Co based FT catalysts. Several similar catalysts have been recently reported: a 3 wt.% Ru/*meso*HZSM-5 exhibited a selectivity of C5-C11 above 70%, together with CH_4 selectivity as low as 7% after 12 h on stream [11, 16]. Exchanging Ru by Co resulted in slightly higher CH_4 and lower C5-C11 selectivities for 8 wt.% Co/*meso*HZSM-5 [9]. Although the performance of the catalysts here presented is somewhat poorer than those systems, it must be stressed that experimental conditions in those works [9, 11, 16] differ from ours: specially the operating pressure (20 bar *versus* 15 bar), time on stream (12 h *versus* 92.5 h), GHSV (2.4 m^3_{STP} kg^{-1}_{cat} h^{-1} *versus* 6 m^3_{STP} kg^{-1}_{cat} h^{-1}), and reactor diameter (7.0 mm *versus* 3.9 mm). Earlier studies have shown that higher operating pressures [17] and lower GHSV [14] normally result in higher chain growth probabilities. At the same time, as the reaction time increases, CH_4 selectivity increases (Fig. 10) for Co/*meso*HZSM-5 catalysts [14]. Indeed, CO conversion and C5-C11 selectivity decreased from 45% and 75% to 36% and 65%, respectively. Unfortunately, for their 8 wt.% Co/*meso*HZSM-5 catalysts no CH_4 selectivity was reported after 107 h on stream [9].

Furthermore, the different preparation method for *meso*HZSM-5 support may also cause a different catalytic performance for Co/*meso*HZSM-5 FT catalysts. After changing the desilication agent from NaOH to TPAOH [7], the surface area of *meso*HZSM-5 increased by 35% and CO conversion increased by 15% while keeping a similar CH_4 selectivity. The higher FT activity in the latter case could be due to a higher cobalt dispersion and the absence of Na species, a well-known poison for Co-based FT catalysts [60]. When a successive acid washing (1 M HNO_3 solution) was performed after the desilication step (1 M TPAOH solution), both the surface area of *meso*HZSM-5 and CH_4 selectivity at iso-conversion conditions increased (from 18.5% to 20%) [14]. This may be ascribed to a higher cobalt dispersion caused by the removal of extra-framework aluminium and the exposure of more hydroxyl groups on the surface of *meso*HZSM-5. The higher CH_4 selectivity reported by Sartipi *et al.* [14] can be attributed to the higher H_2/CO ratio (H_2/CO = 2) used in that study. As it is well known, a higher H_2/CO ratio favours FT reaction towards chain termination [61]. Hence, a larger mesopore surface area in our case compared to that from Wang *et al.* [9] may also lead to

New Journal of Chemistry Accepted Manuscript

a better accessibility of the micropores of the zeolite for cobalt, causing a higher cobalt dispersion and poorer cobalt reducibility, thereby favouring CH_4 formation [8, 17, 56-58].

Co/*meso*HZSM-5 catalysts prepared under stagnant air conditions exhibit higher C5-C11 selectivity (63.8%) than samples pretreated in a gas flow in our experiments. Obviously, the N_2- and NO-pretreated catalysts contain smaller cobalt particles than the samples calcined in air (Fig. 2). This is also confirmed by N_2 adsorption and CO-FTIR results. Considering the presence of the 2063 cm^{-1} band (assigned to CO adsorbed on cobalt in strong interaction with the support [49, 50]), the difference in the intensity of this band for '-stag', '-air' and '-N_2' samples can only be explained by the larger number of small cobalt particles in the latter cases. Despite the fact that air- and N_2-flow pretreatments increase the cobalt reducibility at FT conditions, resulting in more cobalt sites being exposed to the syngas environment, as shown by the much higher intensity of the 2063 cm^{-1} absorbance in Fig. 6b and c, these small reduced cobalt particles can only take part in direct CO hydrogenation and are more easily oxidized in the initial operation period of FT synthesis [14]. Interestingly, compared to the results from Sartipi *et al.*[14], Co/*meso*HZSM-5-stag in our case also shows a higher C5-C11 selectivity (63.8% *versus* 53.5%) and lower C12+ selectivity (10.2% *versus* 18%). Note that these data were collected at a similar CO conversion and the same operating conditions (513 K, 15 bar and H_2/CO = 1), and that the difference between our two catalysts is only the cobalt loading (10.5 wt.% *versus* 23.8 wt.%). Clearly, a good balance between the number of cobalt and acid sites seems to play a key role in the final product distribution for these catalysts. Indeed, the smaller surface area and pore volume in *meso*HZSM-5 for 23.8 wt.%Co/*meso*HZSM-5 than 10.5 wt.%Co/*meso*HZSM-5-stag in the current experiment indicates a more severe pore blocking for the former case, which prevents the contact between the acid sites and hydrocarbons formed from cobalt sites, thereby lowering the hydrocracking intensity.

Thus, the Co particle size distribution and FT activity for Co/*meso*HZSM-5 catalysts are dependent on pretreatment conditions and targeted loading. Co/*meso*HZSM-5 pretreated in gas flows contain more small Co_3O_4 particles than for Co/*meso*HZSM-5 calcined in stagnant air, although large Co_3O_4 particles can also be observed in the air- and N_2-pretreated samples. Unlike results reported for Co/SiO_2 [19, 30] and Co/HZSM-5 [27], a dedicated gas pretreatment resulted for the samples in this study in a decreased FT activity, C5+ selectivity and an increased CH_4 selectivity in comparison with calcination in stagnant air. This lower FT activity and higher CH_4 selectivity are attributed to the lower chain growth probability, a higher hydrogenolysis activity and/or easier oxidation of the present small cobalt particles in these samples.

From the above discussion it has become clear that the choice for the optimal preparation method of bifunctional Co/*meso*HZSM-5 FTS catalysts is strongly dependent on the targeted cobalt loading and mesoporosity of the used support in order to obtain the optimal cobalt particle size for FTS and avoid highly dispersed cobalt. Further for an optimal bifunctionality a fine balance between the number of FTS sites and acid cracking sites is needed together with their accessibility.

Conclusions

In this study, the effect of the pretreatment atmosphere on the structure and catalytic performance of bifunctional Co/*meso*HZSM-5 catalysts in the direct formation of gasoline range hydrocarbons during Fischer-Tropsch Synthesis has been investigated. TEM and TPR results showed that the pretreatment atmosphere influences Co_3O_4 particle size and cobalt reducibility. Pretreatment in a flow of air or N_2 leads to a larger number of small Co_3O_4 particles and a better cobalt reducibility compared with calcination in stagnant air. This can be explained when taking into account that treatment under gas flow suppresses the redistribution of cobalt oxides. NO pretreatment significantly improved cobalt dispersion, while it decreased cobalt reducibility due to the strong interaction between the highly dispersed cobalt oxides or cobalt silicates and *meso*HZSM-5. Given the structure sensitive character of the FTS process, excellent metal dispersion in this case does not lead to a better catalytic performance. Indeed, Co/*meso*HZSM-5-stag exhibited the highest FT activity and C5-C11 selectivity, and the lowest CH_4 selectivity, which is ascribed to the lowest fraction of small cobalt particles. The optimal catalyst preparation method of this bifunctional FTS catalyst depends on the mesoporosity of the zeolite support and the targeted cobalt loading.

Acknowledgements

References

1. E. Iglesia, S. L. Soled and R. A. Fiato, *Journal of Catalysis*, 1992, **137**, 212-224.
2. K. Keyvanloo, M. K. Mardkhe, T. M. Alam, C. H. Bartholomew, B. F. Woodfield and W. C. Hecker, *ACS Catalysis*, 2014, **4**, 1071-1077.
3. J. Lu, L. Yang, B. Xu, Q. Wu, D. Zhang, S. Yuan, Y. Zhai, X. Wang, Y. Fan and Z. Hu, *ACS Catalysis*, 2014, **4**, 613-621.
4. V. P. Santos, T. A. Wezendonk, J. J. D. Jaén, A. I. Dugulan, M. A. Nasalevich, H.-U. Islam, A. Chojecki, S. Sartipi, X. Sun, A. A. Hakeem, A. C. J. Koeken, M. Ruitenbeek, T. Davidian, G. R. Meima, G. Sankar, F. Kapteijn, M. Makkee and J. Gascon, *Nat Commun*, 2015, **6**.
5. E. Iglesia, *Applied Catalysis A: General*, 1997, **161**, 59-78.
6. S. Storsæter, Ø. Borg, E. A. Blekkan and A. Holmen, *Journal of Catalysis*, 2005, **231**, 405-419.
7. S. Sartipi, K. Parashar, M. Makkee, J. Gascon and F. Kapteijn, *Catalysis Science & Technology*, 2013, **3**, 572-575.
8. X. Peng, K. Cheng, J. Kang, B. Gu, X. Yu, Q. Zhang and Y. Wang, *Angewandte Chemie International Edition*, 2015, **54**, 4553-4556.

9. K. Cheng, L. Zhang, J. Kang, X. Peng, Q. Zhang and Y. Wang, *Chemistry – A European Journal*, 2015, **21**, 1928-1937.

10. Q. Zhang, K. Cheng, J. Kang, W. Deng and Y. Wang, *ChemSusChem*, 2014, **7**, 1251-1264.

11. K. Cheng, J. Kang, S. Huang, Z. You, Q. Zhang, J. Ding, W. Hua, Y. Lou, W. Deng and Y. Wang, *ACS Catalysis*, 2012, **2**, 441-449.

12. V. Udaya, S. Rao and R. J. Gormley, *Catalysis Today*, 1990, **6**, 207-234.

13. S. Sartipi, K. Parashar, M. J. Valero-Romero, V. P. Santos, B. van der Linden, M. Makkee, F. Kapteijn and J. Gascon, *Journal of Catalysis*, 2013, **305**, 179-190.

14. S. Sartipi, M. Alberts, V. P. Santos, M. Nasalevich, J. Gascon and F. Kapteijn, *ChemCatChem*, 2014, **6**, 142-151.

15. S. Sartipi, M. Alberts, M. J. Meijerink, T. C. Keller, J. Pérez-Ramírez, J. Gascon and F. Kapteijn, *ChemSusChem*, 2013, **6**, 1646-1650.

16. J. Kang, K. Cheng, L. Zhang, Q. Zhang, J. Ding, W. Hua, Y. Lou, Q. Zhai and Y. Wang, *Angewandte Chemie International Edition*, 2011, **50**, 5200-5203.

17. G. L. Bezemer, J. H. Bitter, H. P. C. E. Kuipers, H. Oosterbeek, J. E. Holewijn, X. Xu, F. Kapteijn, A. J. van Dillen and K. P. de Jong, *Journal of the American Chemical Society*, 2006, **128**, 3956-3964.

18. J. P. den Breejen, P. B. Radstake, G. L. Bezemer, J. H. Bitter, V. Frøseth, A. Holmen and K. P. d. Jong, *Journal of the American Chemical Society*, 2009, **131**, 7197-7203.

19. J. P. den Breejen, J. R. A. Sietsma, H. Friedrich, J. H. Bitter and K. P. de Jong, *Journal of Catalysis*, 2010, **270**, 146-152.

20. Ø. Borg, P. D. C. Dietzel, A. I. Spjelkavik, E. Z. Tveten, J. C. Walmsley, S. Diplas, S. Eri, A. Holmen and E. Rytter, *Journal of Catalysis*, 2008, **259**, 161-164.

21. N. Fischer, E. van Steen and M. Claeys, *Journal of Catalysis*, 2013, **299**, 67-80.

22. A. Martínez and G. Prieto, *Journal of Catalysis*, 2007, **245**, 470-476.

23. A. n. Martínez, C. López, F. Márquez and I. Díaz, *Journal of Catalysis*, 2003, **220**, 486-499.

24. A. Jean-Marie, A. Griboval-Constant, A. Y. Khodakov, E. Monflier and F. Diehl, *Chemical Communications*, 2011, **47**, 10767-10769.

25. J.-S. Girardon, A. S. Lermontov, L. Gengembre, P. A. Chernavskii, A. Griboval-Constant and A. Y. Khodakov, *Journal of Catalysis*, 2005, **230**, 339-352.

26. N. E. Tsakoumis, A. Voronov, M. Rønning, W. v. Beek, Ø. Borg, E. Rytter and A. Holmen, *Journal of Catalysis*, 2012, **291**, 138-148.

27. P. Munnik, N. A. Krans, P. E. de Jongh and K. P. de Jong, *ACS Catalysis*, 2014, **4**, 3219-3226.

28. E. S. Vasiliadou, T. M. Eggenhuisen, P. Munnik, P. E. de Jongh, K. P. de Jong and A. A. Lemonidou, *Applied Catalysis B: Environmental*, 2014, **145**, 108-119.

29. M. Wolters, P. Munnik, J. H. Bitter, P. E. de Jongh and K. P. de Jong, *The Journal of Physical Chemistry C*, 2011, **115**, 3332-3339.

30. J. R. A. Sietsma, J. D. Meeldijk, J. P. den Breejen, M. Versluijs-Helder, A. J. van Dillen, P. E. de Jongh and K. P. de Jong, *Angewandte Chemie*, 2007, **119**, 4631-4633.

31. P. Munnik, P. E. de Jongh and K. P. de Jong, *Journal of the American Chemical Society*, 2014, **136**, 7333-7340.

32. P. Munnik, M. Wolters, A. Gabrielsson, S. D. Pollington, G. Headdock, J. H. Bitter, P. E. de Jongh and K. P. de Jong, *The Journal of Physical Chemistry C*, 2011, **115**, 14698-14706.

33. J. R. A. Sietsma, J. D. Meeldijk, M. Versluijs-Helder, A. Broersma, A. J. v. Dillen, P. E. de Jongh and K. P. de Jong, *Chemistry of Materials*, 2008, **20**, 2921-2931.

34. J. R. A. Sietsma, H. Friedrich, A. Broersma, M. Versluijs-Helder, A. Jos van Dillen, P. E. de Jongh and K. P. de Jong, *Journal of Catalysis*, 2008, **260**, 227-235.

35. J. Landers, G. Y. Gor and A. V. Neimark, *Colloids and Surfaces A: Physicochemical and Engineering Aspects*, 2013, **437**, 3-32.

36. D. Schanke, S. Vada, E. A. Blekkan, A. M. Hilmen, A. Hoff and A. Holmen, *Journal of Catalysis*, 1995, **156**, 85-95.

37. S. Sartipi, H. Jansma, D. Bosma, B. Boshuizen, M. Makkee, J. Gascon and F. Kapteijn, *Review of Scientific Instruments*, 2013, **84**, 124101.

38. D. B. P. J. Van, M. Bracht, G. J. M. Gruter, R. R. de and B. H. Harji, Google Patents2014.

39. R. Caicedo-Realpe and J. Pérez-Ramírez, *Microporous and Mesoporous Materials*, 2010, **128**, 91-100.

40. J. Hong, W. Chu, P. A. Chernavskii and A. Y. Khodakov, *Journal of Catalysis*, 2010, **273**, 9-17.

41. P. Arnoldy and J. A. Moulijn, *Journal of Catalysis*, 1985, **93**, 38-54.

42. G. Prieto, P. Concepción, R. Murciano and A. Martínez, *Journal of Catalysis*, 2013, **302**, 37-48.

43. Ø. Borg, S. Eri, E. A. Blekkan, S. Storsæter, H. Wigum, E. Rytter and A. Holmen, *Journal of Catalysis*, 2007, **248**, 89-100.

44. G. Prieto, A. Martínez, P. Concepción and R. Moreno-Tost, *Journal of Catalysis*, 2009, **266**, 129-144.

45. S. Sun, N. Tsubaki and K. Fujimoto, *Applied Catalysis A: General*, 2000, **202**, 121-131.

46. L. E. S. Rygh and C. J. Nielsen, *Journal of Catalysis*, 2000, **194**, 401-409.

47. L. E. S. Rygh, O. H. Ellestad, P. Klaeboe and C. J. Nielsen, *Physical Chemistry Chemical Physics*, 2000, **2**, 1835-1846.

48. G. Kadinov, C. Bonev, S. Todorova and A. Palazov, *Journal of the Chemical Society, Faraday Transactions*, 1998, **94**, 3027-3031.

49. A. Lapidus, A. Krylova, V. Kazanskii, V. Borovkov, A. Zaitsev, J. Rathousky, A. Zukal and M. Jancˇálková, *Applied Catalysis*, 1991, **73**, 65-81.

50. M. J. Heal, E. C. Leisegang and R. G. Torrington, *Journal of Catalysis*, 1978, **51**, 314-325.

51. H. Xiong, Y. Zhang, K. Liew and J. Li, *Journal of Molecular Catalysis A: Chemical*, 2008, **295**, 68-76.

52. P. Concepción, C. López, A. Martínez and V. F. Puntes, *Journal of Catalysis*, 2004, **228**, 321-332.

53. S. Bessell, *Applied Catalysis A: General*, 1993, **96**, 253-268.

54. E. van Steen, M. Claeys, M. E. Dry, J. van de Loosdrecht, E. L. Viljoen and J. L. Visagie, *The Journal of Physical Chemistry B*, 2005, **109**, 3575-3577.

55. H. Xiong, M. A. M. Motchelaho, M. Moyo, L. L. Jewell and N. J. Coville, *Journal of Catalysis*, 2011, **278**, 26-40.

56. C. Lancelot, V. V. Ordomsky, O. Stéphan, M. Sadeqzadeh, H. Karaca, M. Lacroix, D. Curulla-Ferré, F. Luck, P. Fongarland, A. Griboval-Constant and A. Y. Khodakov, *ACS Catalysis*, 2014, **4**, 4510-4515.

ARTICLE

Journal Name

57. K. Azzam, G. Jacobs, W. Ma and B. Davis, *Catalysis Letters*, 2014, **144**, 389-394.
58. W. Ma, G. Jacobs, Y. Ji, T. Bhatelia, D. Bukur, S. Khalid and B. Davis, *Top Catal*, 2011, **54**, 757-767.
59. R. J. Gormley, V. U. S. Rao, R. R. Anderson, R. R. Schehl and R. D. H. Chi, *Journal of Catalysis*, 1988, **113**, 193-205.
60. A. Y. Khodakov, W. Chu and P. Fongarland, *Chemical Reviews*, 2007, **107**, 1692-1744.
61. R. J. Madon and E. Iglesia, *Journal of Catalysis*, 1993, **139**, 576-590.

Effect of pretreatment atmosphere on the activity and selectivity of Co/mesoHZSM-5 for Fischer-Tropsch Synthesis

Xiaohui Sun,[a] Sina Sartipi,[a] Freek Kapteijn[a] and Jorge Gascon*[a]

a: Catalysis Engineering, Department of Chemical Engineering, Delft University of Technology, Julianalaan 136, 2628 BL Delft, The Netherlands. E-mail: J.Gascon@tudelft.nl; Fax: +31 15 27 89820.

Co/*meso*HZSM-5 pretreatment in different atmospheres changes FT activity and CH_4 selectivity by affecting Co dispersion and reducibility.